Geoscience Frontiers 13 (2022) 101342

HOSTED BY

Contents lists available at ScienceDirect

Geoscience Frontiers

journal homepage: www.elsevier.com/locate/gsf

Research Paper

Partial dehydration of brucite and its implications for water distribution in the subducting oceanic slab

Xinzhuan Guo [a,*], Takashi Yoshino [b], Sibo Chen [c], Xiang Wu [d], Junfeng Zhang [d]

[a] Key Laboratory for High-Temperature and High-Pressure Study of the Earth's Interior, Institute of Geochemistry, Chinese Academy of Sciences, Guiyang 550081, China
[b] Institute for Planetary Materials, Okayama University, Misasa, Tottori 682-0193, Japan
[c] Department of Geosciences, Stony Brook University, Stony Brook, NY 11794-2100, USA
[d] State Key Laboratory of Geological Processes and Mineral Resources, School of Earth Sciences, China University of Geosciences, Wuhan 430074, China

ARTICLE INFO

Article history:
Received 26 July 2021
Revised 21 October 2021
Accepted 21 December 2021
Available online 23 December 2021
Handling Editor: K. Szilas

Keywords:
Partial dehydration
Electrical conductivity
Brucite
Oceanic slab
Water distribution
Hydrous minerals

ABSTRACT

Hydrous minerals within the subducting oceanic slab are important hosts for water. Clarification of the stability field of hydrous minerals helps to understand transport and distribution of water from the surface to the Earth's interior. We investigated the stability of brucite, a prototype of hydrous minerals, by means of electrical conductivity measurements in both open and closed systems at 3 GPa and temperatures up to 1300 K. Dramatic increase of conductivity in association with characteristic impedance spectra suggests that partial dehydration of single-crystal brucite in the open system with a low water fugacity occurs at 950 K, which is about 300 K lower than those previously defined by phase equilibrium experiments in the closed system. By contrast, brucite completely dehydrates at 1300 K in the closed system, consistent with previous studies. Partial dehydration may generate a highly defective structure but does not lead to the breakdown of brucite to periclase and water immediately. Water activity plays a key role in the stability of hydrous minerals. Low water activity (aH_2O) caused by the high wetting behavior of the subducted oceanic slab at the transition zone depth may cause the partial dehydration of the dense hydrous magnesium silicates (DHMSs), which significantly reduces the temperature stability of DHMS (this mechanism has been confirmed by previous study on super hydrous phase B). As a result, the transition zone may serve as a 'dead zone' for DHMSs, and most water will be stored in wadsleyite and ringwoodite in the transition zone.

1. Introduction

Water can be stored in the lattice site of hydrous minerals, as well as in nominally anhydrous minerals (NAMs) as H-related point defects such as OH groups. Dehydration of hydrous minerals releases water and consequently affects a number of physicochemical properties of the mantle, such as electrical conductivity (Chen et al., 2018), viscosity (Nakao et al., 2016) and rheology (Behr et al., 2018), mantle wedge dynamics (Arcay et al., 2005), and earthquakes (Ferrand et al., 2017). Therefore, it is of great importance to identify the stability field of hydrous minerals and their dehydration process. The stability fields of hydrous minerals are traditionally defined by either in situ techniques (e.g., X-ray diffraction (XRD), Raman spectroscopy) or quench experiments (Schramke et al., 1982; Kanzaki, 1991; Fei and Mao, 1993; Shinoda et al., 2002; Ma et al., 2013). Alternatively, electrical conductivity measurement of hydrous minerals under high pressure and temperature conditions is useful to monitor the dehydration process because electrical conductivity is very sensitive to fluid component with highly mobile ion (Manthilake et al., 2015, 2016; Li et al., 2016; Hu et al., 2017; Chen et al., 2018; Zhang et al., 2021).

Previous studies have shown that electrical conductivity of hydrous minerals always promptly increases at temperatures far below (at least 100–200 K) the well-known dehydration temperature (e.g., brucite: Fuji-ta et al., 2007; Gasc et al., 2011; amphibole: Wang et al., 2012; Hu et al., 2018; serpentine and dense hydrous magnesium silicates (DHMS): Guo et al., 2011; Guo and Yoshino, 2013). However, texture observations of the recovered samples have not shown clear evidence for the breakdown of these hydrous minerals. Origin of the conductivity jump is still in debate. For example, it has been suggested that the conductivity jump observed at 800 K and 1 GPa could be explained as the dehydration

* Corresponding author.
E-mail address: gxzhuan@mail.gyig.ac.cn (X. Guo).

https://doi.org/10.1016/j.gsf.2021.101342

of amphibole associated with the oxidation of iron. However, for Fe-free samples (e.g., brucite) a more reasonable explanation for the conductivity change within its stability field might be the effect of water released from partial dehydration of brucite (Fuji-ta et al., 2007). All the above experiments did not focus on the partial dehydration process and its mechanism, and did not discuss its important implications for water distribution in the Earth's interior.

To address the above questions, we carried out in situ electrical conductivity measurements on brucite, the simplest hydrous mineral, at 3 GPa and temperatures up to 1300 K in both open and closed systems. Brucite ($Mg(OH)_2$), space group: $P\bar{3}m1$, is chosen as a prototype of hydrous minerals, in which (MgO_6) octahedral are linked together by sharing edges to form a (MgO_6) octahedral layer stacking along the *c*-axis. Brucite is stable in a wide *P-T* conditions (Fei and Mao, 1993), whose natural form has been found in the depth at least to the top of the lower mantle (Palot et al., 2016). Brucite also plays an important role in producing olivine and transporting water, the major mineral in the mantle, through the reaction brucite + antigorite = olivine + chlorite + water (Kempf and Hermann, 2018; Peters et al., 2020). Due to its importance in water transporting, its simplicity in chemistry and structure, brucite is the best starting material to monitor dehydration process of hydrous minerals. Based on the characteristic impedance spectra and post-experimental analysis of the recovered samples, we propose that partial dehydration does occur when the water activity is low. Thus, water activity (aH_2O) plays an important role in driving the dehydration process for hydrous minerals. The water activity is closely related to the wetting behaviors of the rocks of interest.

It has been proved that the transition zone is at least locally water enriched through the discovery of natural H_2O-riched ringwoodite (Pearson et al., 2014) and the experiments of dehydration melting of ringwoodite together with the seismic data (Schmandt et al., 2014). How is water transported into the transition zone, what is the water carrier, and how does water distribute in the deep Earth's interior down to the transition zone? To clarify these questions, we further discussed them in the scope of characteristic changes of wetting behavior with *P-T* conditions in the subducting slab.

2. Experimental methods

2.1. Sample preparation

Natural single-crystal $Mg(OH)_2$ and hot-pressed polycrystalline $Mg(OH)_2$ were used as the starting materials for electrical conductivity measurements. Microstructural observations by a Quanta2000 field emission gun scanning electron microscope (FEG-SEM) with an accelerating voltage of 15 kV, a beam current of 20 nA, and a beam size of 5 μm, indicated that there were no inclusions and minor phases in the natural single crystal. The chemical compositions of brucite were analyzed using a JEOL-8100 electron microprobe with an accelerating voltage of 15 kV, a beam current of 20 nA, and a beam size of 3 μm. Olivine and hematite were used as standards for Mg and Fe, respectively. Both the FEG-SEM and EPMA are installed at the State Key Laboratory of Geological Processes and Mineral Resources, China University of Geosciences (Wuhan). Chemical composition analysis showed that the brucite crystal is almost pure in $Mg(OH)_2$, with the FeO content less than 0.1 wt.%. A Laue camera, with the characteristic K_α X-ray of Mo, was used to determine the crystallographic orientation of the single crystal. As cleavages are likely to develop along the (001) plane in a brucite crystal we carefully chose parts of the crystal without cracks under the optical microscope. The single crystal was cored to a cylindrical shape with 2 mm in diameter, with an axis parallel to (001) using an ultrasonic drilling machine. Then the single crystal was double-polished to 0.5 mm in thickness. The polycrystalline $Mg(OH)_2$ was prepared by sintering the $Mg(OH)_2$ powder at 1200 K and 3 GPa using a DIA-type high-pressure apparatus for 2 h. The cell design is the same as that used in Guo and Yoshino (2014) except that an unsealed Mo capsule was used instead of a Pt capsule. Then the hot-pressed brucite was cored to a cylindrical shape with a diameter of 2 mm and a thickness of 0.5 mm using an ultrasonic drill. All the samples were kept in a vacuum furnace at 473 K before the conductivity measurements to avoid absorbing water from the air.

2.2. Cell design

Two types of high-pressure presses, including Kawai-type multianvil press installed at Okayama University and a Walker-type press installed at China University of Geosciences (Wuhan) were used for conductivity measurements in this study. A pre-sintered Cr_2O_3-bearing MgO octahedron with an edge length of 25 mm was used as the pressure medium. For conductivity measurements in an open system for water, polycrystalline MgO was used as capsules, and two Mo disks were used as electrodes. For conductivity measurements in a closed system, the starting material was enclosed in the single-crystal quartz sleeve and sandwiched by two Pt-Mo (Pt with a thickness of 0.1 mm and Mo disk with a thickness of 0.5 mm) electrodes. The sample was sealed by Pt foil and single-crystal quartz during compression to avoid escape of water (Guo et al., 2015; Li et al., 2018). Two sets of WRe_5-WRe_{26} thermocouples were used to monitor the temperature. Eight tungsten carbide cubes with a truncated edge length of 15 mm were used as the second stage anvils. The detailed cell design and pressure calibration of cell assembly for the Walker-type press were described in Li et al. (2018). The temperature gradient within the heater is around 10–20 K/mm. The temperature difference between the surface and the center of the sample is less than 5 ℃ in case of a sample with a thickness of 0.5 mm.

2.3. Electrical conductivity measurements

Impedance spectra of the sample were measured using a Solartron 1260 impedance Gain-Phase analyzer combined with a Solartron 1296 dielectric interface, operating with 1 V alternating current at frequencies from 1 M to 0.1 Hz. The electrical conductivity (σ) is calculated from $\sigma = \frac{l}{SR}$, where l is the sample length, S is the cross-section area of the sample, and R is the resistance of the sample.

Conductivity measurements were performed at pressure of 3 GPa and temperatures between 500 K and 1300 K. Before the conductivity measurements, the cell assembly was kept in a vacuum furnace at 395 K to eliminate the absorbed water. A typical conductivity measurement was conducted as below. At 3 GPa, the sample was first heated to 750 K and kept for several hours until the sample's resistance stabilized to preclude the absorbed water effect. Then we heated the sample to the desired temperature (1000 K for partial dehydration experiments, and 1300 K for dehydration experiments, referred to Kanzaki (1991)), finally cooled to the lowest temperature (500–600 K) at which we could measure the impedance spectra with high signal-to-noise ratio. The temperature change was set at 50 K or 100 K interval in the heating cycle and 25 K interval in the cooling cycle, and the impedance spectra were simultaneously acquired. In some runs, an extra heating cycle using step-wise temperature increment was also conducted to confirm the data reproducibility. The conductivity data acquired in the cooling cycle were used to calculate the activation enthalpy and the preexponential factor. The experimental conditions and results are shown in Table 1.

Table 1
Experimental conditions and results.

Run No.	Starting material	P (GPa)	T (K)	σ_0 (S/m)	H (eV)	Capsule
R694	Brucite (//c axis)	3	650–900 (before dehydration)	0.84	0.65	MgO[a]
			600–1000 (partial dehydration)	0.96	0.024	
R720	Brucite (//c axis)	3	500–900 (before dehydration)	9.4	0.53	SiO_2[b]
			600–1300 (after dehydration)	1.55	0.15	
1 k1398	Brucite (//c axis)	3	550–750	1.11	0.72	MgO[a]
1 k1321	Brucite (Poly.)	3	550–750	149.6	0.9	MgO[a]

[a] When polycrystalline MgO was used as the capsule, the system is open for water.
[b] When single-crystal quartz was used as the capsule, two Pt-Mo electrodes were also used to prevent water escaping. In this case, the system is regarded as a closed system.

After the conductivity measurements, the recovered samples were analyzed in FEG-SEM with both secondary electron image (SEI) and backscattered electron image (BEI) installed at China University of Geosciences (Wuhan). The phases of the different run products and micro-structures were confirmed using a D/MAX Rapid X-ray diffractometer installed at Central South University, China, which is operated with a voltage of 40 kV, a beam current of 80 mA and a beam size of 5 μm. The micro-structure of partially dehydrated sample was checked using a transmission electron microscope (TEM) (JEOL JEM-2010 at N-BARD of Hiroshima University, Japan) with an accelerating voltage of 200 kV.

3. Results

Fig. 1a shows the logarithmic electrical conductivity of single-crystal brucite along the *c*-axis as a function of reciprocal temperature in an open system (R694). In this experiment, polycrystalline MgO was used as the sample capsule, so that the system can be regarded as an open system for water. The sample was firstly sintered at 750 K for 7 h to preclude the absorbed water within the sample capsule. When the sample was heated to around 950 K a quick increase in conductivity was observed. The sample was further heated to 1000 K, and the sample's conductivity continuously increased within 40 min (Fig. 1b). The absolute conductivities increased about 3 orders of magnitude. The fast and robust conductivity rise above 950 K may indicate a dehydration process similar to the dehydration of phengite (Chen et al., 2018). The electrical conductivities and temperatures were fitted to the Arrhenian equation,

$$\sigma = \sigma_0 \exp\left(-\frac{\Delta H}{kT}\right) \quad (1)$$

where σ_0 is the preexponential factor (S/m), T is the absolute temperature (K), k is the Boltzmann constant (J/K), and ΔH is the activation enthalpy (eV). The activation enthalpies of conductivity determined before and after dehydration were 0.65 eV and 0.024 eV, respectively. Consistency between the final heating path and previous cooling path indicates a slow drain rate of the MgO capsule used in this run.

Fig. 2 shows the logarithmic electrical conductivity of single-crystal brucite along the *c*-axis as a function of reciprocal temperature in a closed system (R720). In this experiment, single-crystal quartz and two Pt foils were used to prevent water loss. The water initially absorbed by the sample could not be excluded from the cell assembly. As a result, the conductivities were enhanced more than 2 orders of magnitude at temperatures lower than 900 K by the absorbed water and the conductivity is almost independent of temperature. We did not observe the dehydration process up to 1000 K as shown in R694. The electrical conductivity increases

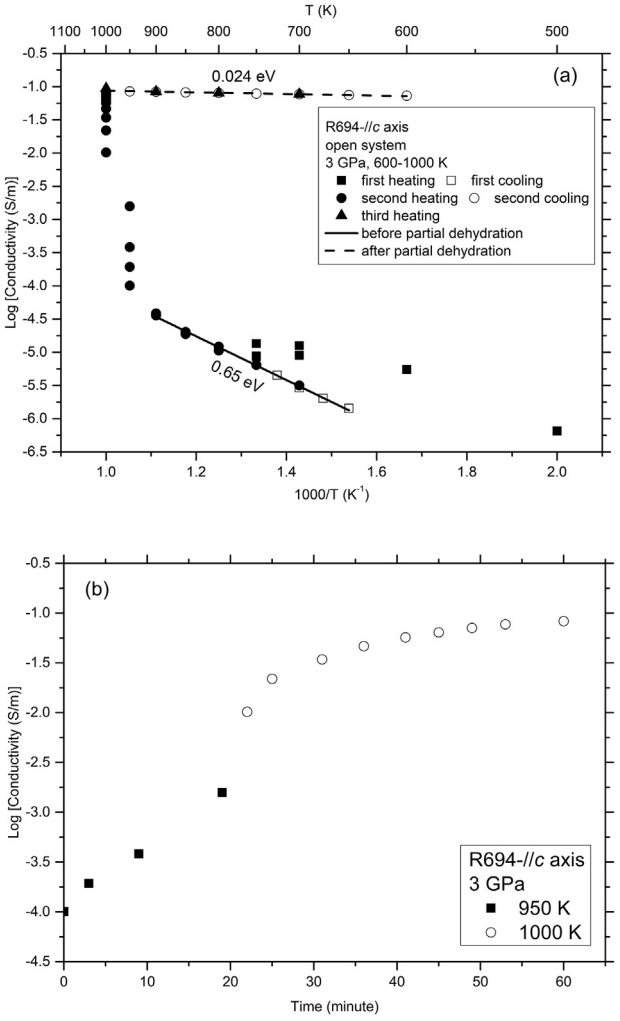

Fig. 1. Electrical conductivity of single-crystal brucite along *c*-axis in terms of temperature and time. (a) Electrical conductivity of brucite in an open system (R694). The activation enthalpies before and after the partial dehydration are labeled. Partial dehydration strongly enhances the conductivities from 950 K. (b) Electrical conductivity changes with time. The electrical conductivity was enhanced more than 3 orders of magnitude within 1 h.

with temperature since 1000 K. To confirm the partial dehydration the electrical conductivity was measured at least two times within 10 min at each temperature. If partial dehydration occurs, the electrical conductivity will quickly increase. However, the conductivity usually keeps constant or just slightly increases. The activation

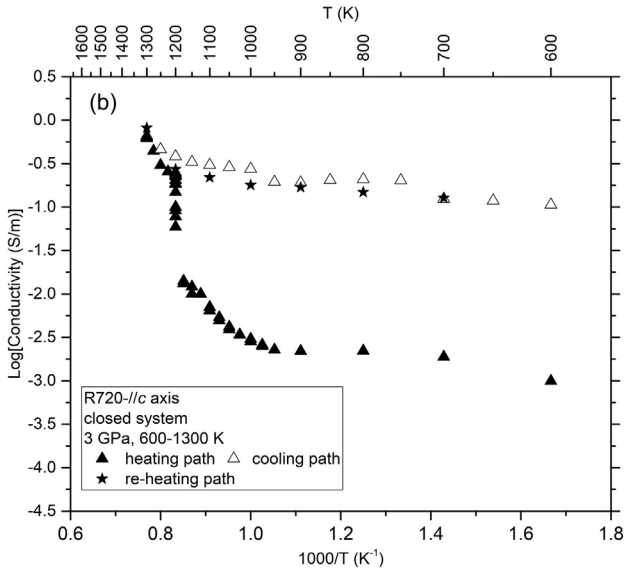

Fig. 2. Logarithmic electrical conductivity of single-crystal brucite along *c*-axis at temperatures up to 1300 K in a closed system (R720). The initial high conductivities before dehydration of brucite may be caused by the absorbed water within the assembly.

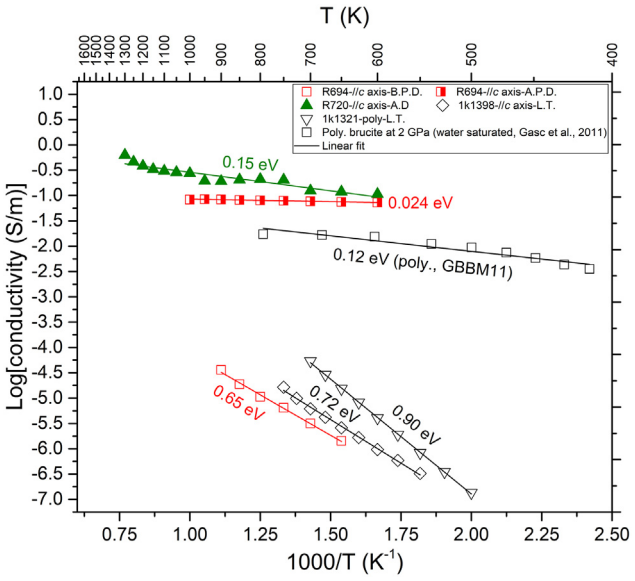

Fig. 3. Comparison of the conductivities of brucite before and after its partial dehydration or complete dehydration. Note: B.P.D., before partial dehydration; A.P.D., after partial dehydration; A.D., after dehydration; L.T., low temperature; poly., polycrystalline; GBBM11, Gasc et al. (2011).

enthalpy is around 1.1 eV from 1000 K to 1150 K, much higher than those after partial dehydration (R694). Therefore, the slow increase of conductivity at 1000–1150 K is just temperature dependent. The conductivity significantly increased above 1200 K, indicating the onset of final dehydration at 1200 K. To completely dehydrate the brucite crystals, we further increased the temperature to 1300 K. During cooling below 1300 K the conductivities were nearly independent of temperature. The activation enthalpy determined from the path after the dehydration of brucite is 0.15 eV, close to that of protonic conductivity in de-ionized water (e.g., 0.1–0.15 eV; Zheng et al., 1997). The low activation enthalpies of partial or completely dehydrated sample indicate that the high conductivities are attributed to the fluid phase (water).

To evaluate the data quality, we conducted two extra measurements at temperatures lower than 750 K for the starting materials of single-crystal (// *c*-axis, 1 k1398) and polycrystalline $Mg(OH)_2$ (1 k1321). In these two experiments, the cell design is completely the same as that used in R694 (Table 1). As shown in Fig. 3, the conductivities of single-crystal brucite along the *c*-axis from two different experiments are almost consistent with each other at temperatures below 900 K. The bulk conductivities of the dehydrated brucite in the closed system (R720) are relatively higher than those of brucite under water-saturated conditions (Gasc et al., 2011) and those of partially dehydrated brucite (R694) measured in an open system for water. The conductivities and activation enthalpy of polycrystalline brucite are slightly higher than those of single-crystal brucite along the *c*-axis because the polycrystalline brucite represents averaged conductivities and activation enthalpy of an anisotropic conductivity feature of brucite (Guo and Yoshino, 2014).

4. Discussions

4.1. Dehydration process inferred from electrical conductivity measurements

Representative impedance spectra of brucite (R694) before its dehydration contained a single semicircle at high frequencies as well as a small "tail" at low frequencies (Fig. 4a). The impedance arc can be well fitted to an equivalent circuit composed of a resistance (*R*) and a capacitance (*C*) in parallel. The fitting error is less than 2%. When dehydration occurred (e.g., 1000 K), the impedance arc quickly and strongly shrank at low frequencies during one spectra-collection (~2 min). Because the characteristic impedance spectral shape caused by dehydration could not allow fitting to the *R-C* equivalent circuit in parallel to determine the sample resistance, the resistance at the lowest frequency (0.1 Hz) was adopted as the sample resistance instead (Fig. 4b). After 1-hour partial dehydration, the impedance spectra only contained one-quarter impedance arc in a measured frequency range, which were also fitted by the *R-C* equivalent circuit in parallel (Fig. 4c). Characteristic impedance spectra of R694 (Fig. 4b) strongly suggest that the dehydration of brucite occurred at temperatures above 950 K. By contrast, the dehydration temperature of brucite aggregates defined by quench method in a closed system at 3 GPa is around 1350 K (Irving et al., 1977) and it in-situ observed by differential thermal analysis in a closed system at 3 GPa is about 1273 K (Kanzaki, 1991).

Fig. 5 shows the back-scattered images (BSIs) of the recovered sample of R694. Only the brucite phase can be identified. The sharp boundary between the sample and the MgO capsule was kept without evidence of reaction. The micro-focused X-ray diffraction patterns of the recovered samples also indicated that brucite did not decompose to periclase and water. The crystal morphology and composition differences of the starting materials, together with uncertainties in *P-T* estimations are not likely to explain the huge gap in dehydration temperatures between the phase equilibrium experiments and this study. We propose that partial dehydration occurs within the stability field of brucite during the conductivity measurement. Such kind of dehydration may have generated the defective structure, $Mg(OH)_{(2-x)}O_{x/2}D_{x/2}$ ($x < 2$; D, the Schottky-Frenkel vacancy pairs at –OH site; see Freund and Wengeler, 1980); nevertheless, the crystal structure of brucite did not collapse within the experimental duration.

In contrast, complete dehydration of brucite at 1300 K led to the breakdown of brucite in a closed system (Fig. 6, R720). The texture showed that part of brucite remained in the center of the sample. It is likely that brucite dehydrated first from the surface. The

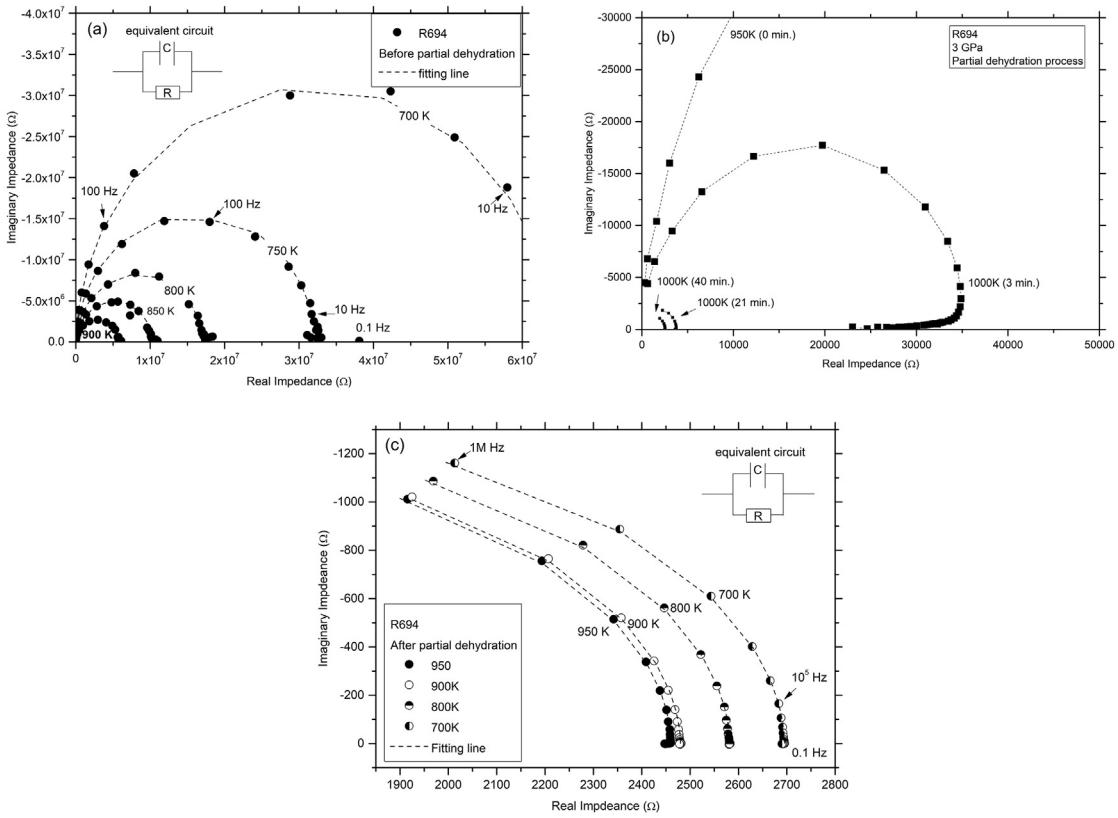

Fig. 4. Representative impedance spectra of single-crystal brucite along *c*-axis. (a) The impedance spectra before partial dehydration of brucite. The dashed lines denote the fitting result using the equivalent circuit composing a capacitance and a resistance in parallel. (b) The impedance spectra during the partial dehydration process. Impedance arcs strongly shrink during one data-collecting period (~2 min). (c) The impedance spectra collected during cooling from 1000 K. After partial dehydration of 1 h, the impedance arcs no more strongly shrink, and the temperature dependence of conductivities is weak. The dashed lines denote the fitting result using the equivalent circuit composing a capacitance and a resistance in parallel.

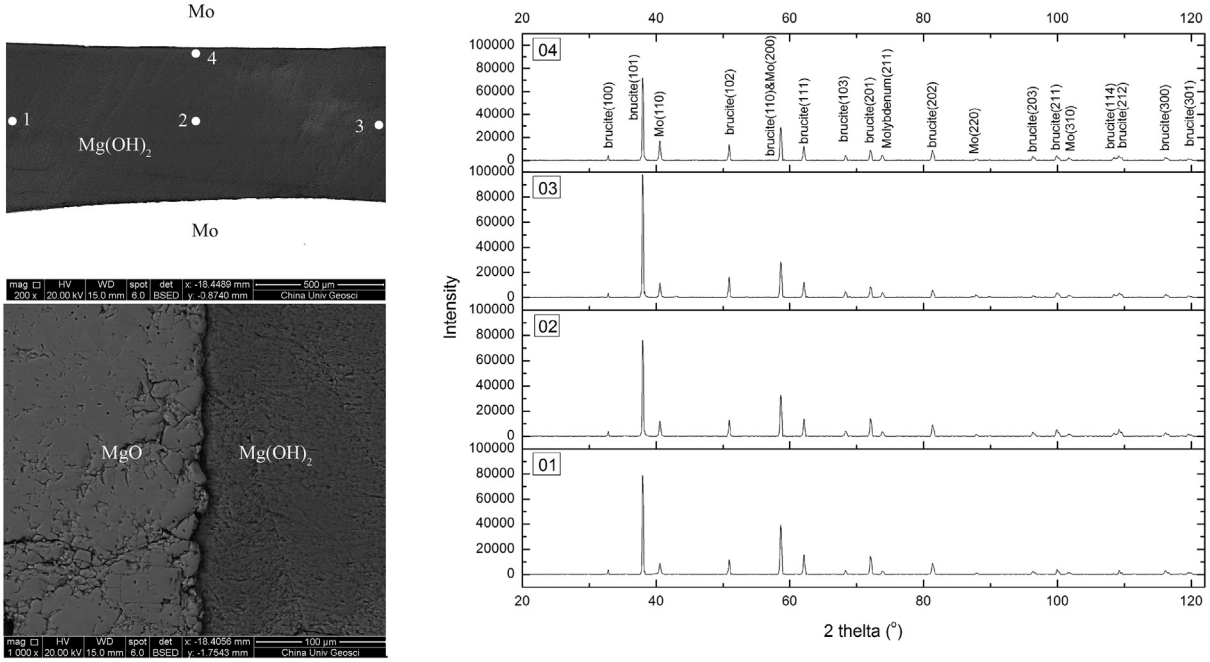

Fig. 5. Texture observations and XRD patterns of the recovered sample of R694. Only one phase can be observed for the sample. No reaction rim can be recognized between MgO capsule and $Mg(OH)_2$ sample. The relative bright part is brucite may be contaminated by Mo during polishing the sample. Four points of single-crystal brucite were checked by micro-focused XRD. Points 1 and 3 are very close to the boundary between the MgO capsule and the sample. No diffraction peaks of periclase can be identified, indicating the crystal structure of brucite does not collapse after partial dehydration of 1 h.

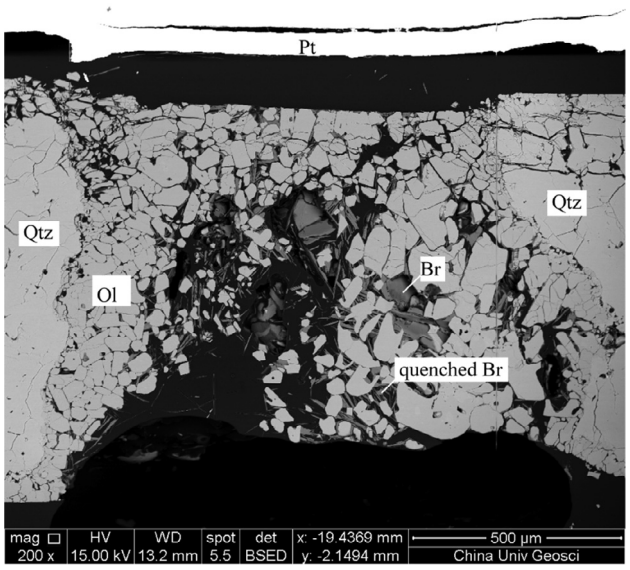

Fig. 6. The back scattered image of the recovered sample of R720. Part of single-crystal brucite does not decompose, indicating the dehydration process of brucite starts from the crystal surface. Needle-like brucite was formed during quenching the sample. Abbreviations: Ol, Olivine; Qtz, Quartz; Br, Brucite; Pt, Platinum.

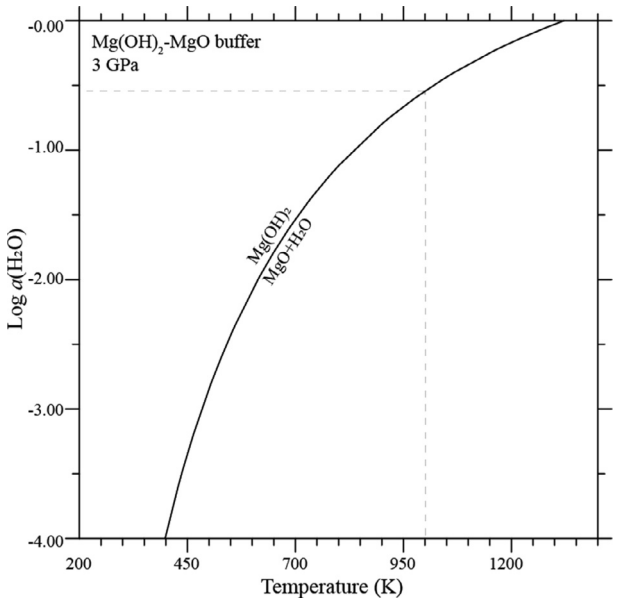

Fig. 7. Water activity buffered by MgO-$Mg(OH)_2$ as a function of temperature at 3 GPa. Theriak-Domino software is used for calculation. The water activity is as low as 0.28 when single-crystal brucite partially dehydrated at 1000 K.

dehydrated products (MgO + H_2O) reacted with SiO_2 capsule to produce Mg_2SiO_4. This reaction initiated from the boundary between quartz and brucite and progressively towards the center part. The needle-like brucite was formed during quenching in the liquid phases (including water and dissolved MgO component). These observations and explanation are consistent with the observations by van Aken and Langenhorst (2001) who reported the in-situ dehydration process of single-crystal brucite, in which experiment the dehydration started from the rim of hexagonal brucite plates and proceeded towards the core. Dehydration of brucite in this study should also start from the surface of the sample, leaving a defective structure at the surface filled by water. It is expected that the defective structure accumulates with time in a low kinetics and will eventually cause the breakdown of brucite.

4.2. Influence of H_2O activity on the dehydration process of hydrous minerals

For R694, the use of MgO capsule together with $Mg(OH)_2$ sample in R694 buffers the water activity (aH_2O) due to the reaction:

$$Mg(OH)_2 = MgO + H_2O \quad (2)$$

Under equilibrium conditions, the Gibbs free energy of reaction (2) is

$$\Delta G_{T,P} = \Delta G_0(T,P) + RT \cdot \ln(aH_2O) = 0 \quad (3)$$

where $\Delta G_0(T,P)$ is the standard state Gibbs free energy of reaction (2) at certain T and P. The calculated water activity (Fig. 7) buffered by $Mg(OH)_2$-MgO at 3 GPa and 1000 K is as low as 0.28 using the Theriak-Domino software (de Capitani and Petrakakis, 2010). The use of single-crystal quartz and two Pt foils in R720 can constitute a closed system (Guo et al., 2015). The moisture enclosed within the capsule can efficiently increase the aH_2O. Partial dehydration at 1000 K in R720 was not observed. Even if partial dehydration of brucite initially occurred at 1000 K, which could lead to water release and in turn cause the increase of aH_2O to suppress the further dehydration process.

Dehydration of brucite in an open system at lower temperatures relative to the phase equilibrium experiments can be explained by the low aH_2O characteristic of our experiments. Dehydration experiments on antigorite in an open system using the in-situ X-ray diffraction technique (Perrillat et al., 2005) also clearly demonstrated that the temperature stability of antigorite decreased by 50–100 K and the dehydration rates are much faster than those reported for water-saturated conditions. Their results indicate that aH_2O is a strong driving force for dehydration. Furthermore, infrared synchrotron radiation study of brucite (Shinoda et al., 2002) showed that proton becomes highly active and does not occupy a specific crystallographic site under high temperature and pressure conditions within the stability field of brucite. Consequently, some water may escape easily from the structure and form on the surface of brucite under low aH_2O conditions. We suppose that partial dehydration of brucite will be a continuous process until the breakdown of its crystal structure with time if the low aH_2O can be sustained.

Another situation has to be considered to explicate the partial dehydration. Small cavities in interstitials of brucite single crystal may induce locally lower pressure than the confining pressure because crystal itself serves as the skeleton for cavities. This mechanism has been used for the segregation and migration of melt from peridotite to diamond aggregates (Hirose and Kushiro, 1993). Consequently, the dehydration temperature around the cavities may be lower than the values defined by phase equilibrium experiments. However, the rapid conductivity jump can only be realized by the scenario that the dehydrated fluids are interconnected within the crystal. This requires the relatively homogeneous distribution of cavities within the crystal and the dehydrated fluids are interconnected. Nano-scale observation by the transmission electron microscope on the starting material carried out at Hiroshima University did not support the homogeneously distributed cavities in the samples (Fig. 8). Therefore, cavities induced partial dehydration at lower temperature is unlikely to occur in our experiments.

4.3. Implications for water distribution within the subducting oceanic slab

The dehydration of brucite at temperatures below the previously determined ones (about 300–400 K lower) has been documented by the electrical conductivity measurements (Fuji-ta

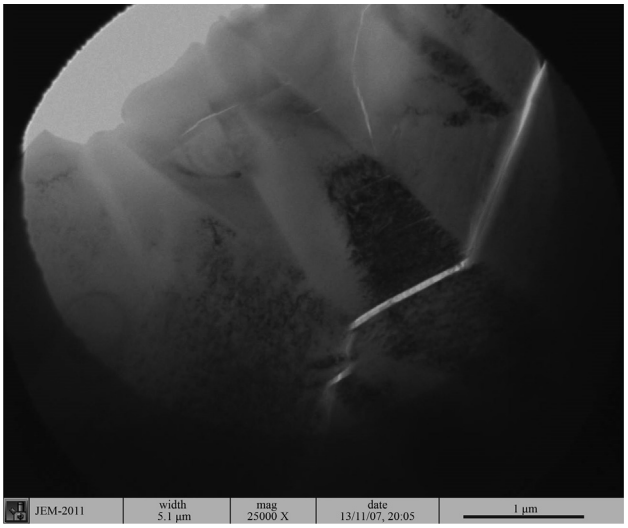

Fig. 8. Nano-scale observation by the transmission electron microscope on the starting material of brucite single crystal. No homogeneously distributed cavities can be observed.

et al., 2007; Gasc et al., 2011). Both their studies have shown that the electrical conductivity increased after the onset of dehydration. Recently, Hu et al. (2018) reported a continuous and remarkable increase of conductivity of single-crystal amphibole at 873 K. Similarly, Wang et al. (2012) reported a rapid increase of the electrical conductivity of plagioclase-bearing amphibolite above 800 K. The changes in conductivity might be caused by onset of the partial dehydration of amphibole below the dehydration temperature. Guo et al. (2011) and Guo and Yoshino (2013) reported the conductivity enhancement of serpentine and super hydrous phase B (one of DHMSs) at temperatures within their stabilities which was also likely caused by partial dehydration. All of these experiments were conducted in the open system for water, which yields a low aH_2O. Therefore, partial dehydration might be ubiquitous for hydrous minerals at temperatures 100–200 K below their stabilities because the aH_2O in an open system is low, irrespective of their crystal structures, water contents, mineral chemistry and the prevailing P and T. The difference is just how much lower the partial dehydration temperatures than the values defined by the phase equilibrium experiments in a closed system.

In the subducted slab, water is mainly stored in hydrous minerals and NAMs. Whether the released water can be maintained in the subducted slab depends on the wetting behavior of the peridotite-water system and the overlying basalt-water system. If the dihedral wetting angle (θ) is smaller than 60°, the grain edge channels remain open, while if $\theta > 60°$ they will close off and the fluids will be trapped in the grain corners. The dihedral angle of fluid-olivine-olivine ($\theta_{\text{fl-Ol-Ol}}$) significantly decreases with increasing P–T condition (Watson et al., 1991; Mibe et al., 1998; Mibe et al., 1999; Yoshino et al., 2007) for peridotite part of the subducting slab, indicating that the released water through the breakdown of hydrous minerals can form interconnected network. However, whether the released water can move upward to wet the mantle wedge depends on the wetting behavior in the subducting oceanic crust, which is controlled by $\theta_{\text{fl-Cpx-Cpx}}$, $\theta_{\text{fl-Cpx-Grt}}$, and $\theta_{\text{fl-Grt-Grt}}$. For a hot slab, the $\theta_{\text{fl-Grt-Grt}}$ is always lower than 60° at depth (Ono et al., 2002; Mibe et al., 2003; Matsukage et al., 2017; Liu et al., 2018; Fig. 9). The reduced stability of hydrous minerals due to the partial dehydration in an open-system will facilitate the water loss from the subducting oceanic slab, and most released water from the breakdown of hydrous minerals will penetrate the oceanic crust and wet the overlying mantle wedge.

As for a cold slab, $\theta_{\text{fl-Cpx-Cpx}}$, $\theta_{\text{fl-Cpx-Grt}}$, and $\theta_{\text{fl-Grt-Grt}}$ are all larger than 60° (Ono et al., 2002; Mibe et al., 2003; Matsukage et al., 2017; Liu et al., 2018). Therefore the closed system in the oceanic crust can be sustained before the slab subducting into the transition zone. The aqueous fluids released through the breakdown of hydrous minerals, e.g., lawsonite, phengite, and serpentine, could be trapped as interstitial fluids in the oceanic crust, although these fluids can flow freely on the grain edges in the peridotite part of the slab. Partial dehydration of hydrous minerals in the oceanic crust will in turn increase aH_2O of the system to unity. As a result, the complete dehydration will be restrained. The stability field of hydrous minerals is consistent with that under water-saturated conditions. We should note that the shear deformation introduced through plate movement and mantle convection could change the pore geometry and further influence the interconnection of the crustal and mantle rocks (Holtzman et al., 2003; Zhang et al., 2014). As a result, partial dehydration of hydrous minerals may also occur locally in a cold subducting slab.

When the cold oceanic slab is subducted into the transition zone, partial dehydration of dense hydrous magnesium silicates (DHMS) in the peridotite layer likely occurs for three reasons: (1) Better wetting behavior of oceanic crust ($\theta_{\text{fl-Grt-Grt}}$ less than 60°, Fig. 9) and therefore low water activity; (2) Higher temperature of the subducted slab, especially when the slab becomes stagnant in the transition zone; (3) Previous experiments have confirmed the partial dehydration of super hydrous phase B under the conditions of low water activity and low temperatures (Guo and Yoshino, 2013). Aqueous fluids, including those physically trapped in the slab and those formed lately through partial dehydration of hydrous minerals will eventually segregate from the subducted slab and hydrate the transition zone. The partial dehydration mechanism for the hydrous minerals inevitably cause the disappearance of DHMSs, such as phase E, super hydrous phase

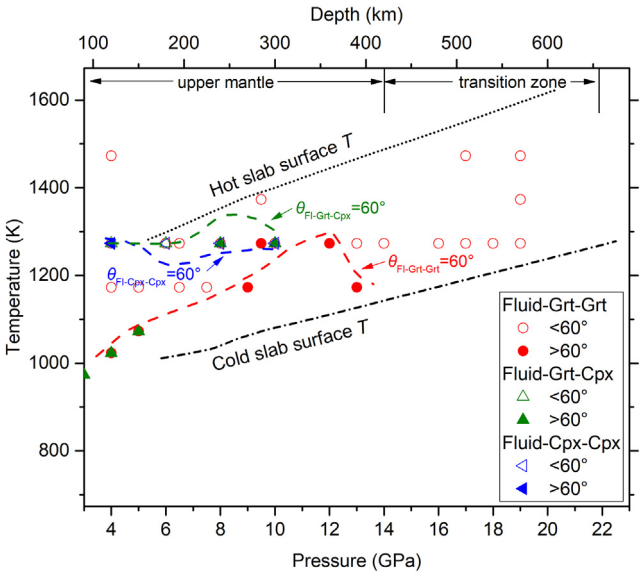

Fig. 9. The Fluid-Grt-Grt, Fluid-Grt-Cpx, and Fluid-Cpx-Cpx dihedral angles as functions of pressure (GPa) and temperature (K), modified from Liu et al. (2018). If the dihedral wetting angle (θ) is smaller than 60°, the grain edge channels remain open (the system can be regarded as an open one), while if $\theta > 60°$ they will close off and the fluids will be trapped in the grain corners (the system can be regarded as a closed one). The open symbols present denote the dihedral angles smaller than 60° and greater than 60°, respectively. The $\theta_{\text{Fl-Grt-Grt}}$ data are from Mibe et al. (2003), Ono et al. (2002), Matsukage et al. (2017), and Liu et al. (2018). The $\theta_{\text{Fl-Grt-Cpx}}$ data are from Matsukage et al. (2017), Mibe et al. (2003). The $\theta_{\text{Fl-Cpx-Cpx}}$ data are from Matsukage et al. (2017). The dotted and dash-dotted black lines represent the global range of slab surface temperature, extrapolated from Syracuse et al. (2010). Abbreviations: Fl, Fluid; Grt, Garnet; Cpx, Clinopyroxene.

B, and phase D, under the transition zone condition. Therefore, we propose that the transition zone serves as a 'dead zone' for DHMSs. Someone may notice that brucite (wave number 3698 cm^{-1}) coexists with natural hydrous ringwoodite in the study of Pearson et al. (2014). It may be argued that at least brucite is stable and can coexist with ringwoodite at depths between 520 km and 660 km in the transition zone. We think that brucite is not formed in-situ together with ringwoodite at depth despite brucite itself is stable at the depth of transition zone with a geotherm lower than 1500 K (Fei and Mao, 1993). According to the phase equilibrium experiments on MSH system, brucite only occurs in association with phase D and liquid at very low temperature (<1173 K) at the bottom of the transition zone if the Mg/Si = 1 and the water content is as high as 15 wt.% for the starting materials (Ohtani et al., 2001). Alternatively, in a locally Mg-rich (a low Si activity) and water rich environment, hydrous ringwoodite (water content higher than 1.5 wt.%, near the maximum water solubility of 2.5 wt.%) is formed at depth. It was then captured through in situ diamond formation. In the following fast exhumation of diamond from the deep interior, small amount of water will be released from ringwoodite to form MgO-riched fluid first corresponding to the positive pressure effect on the water solubility of ringwoodite. When the *P–T* condition falls within the stability field of brucite, brucite will be formed. The formation kinetics of brucite from H_2O and MgO is very fast, which is common during the quenching of MgO-rich fluid under high *P–T* conditions. The formation mechanism is somewhat like the formation of brucite on the surface of natural periclase from the top of the lower mantle (Palot et al., 2016).

The direct implication of partial dehydration of hydrous minerals is to explain the high conductivity anomalies revealed by magnetotelluric data. For example, the origin of the high conductivity anomalies in the region relevant to the subduction zone was explained by the dehydration of hydrous minerals (chlorite, Manthilake et al., 2016; lawsonite, Manthilake et al., 2015; phengite, Chen et al., 2018). If partial dehydration of these minerals prevails under the condition of low water activity, the dehydration temperature defined by MT data, geotherm, and stability field (determined by phase equilibrium in a closed system) might be largely overestimated on a geological time scale.

5. Conclusions

Low water activity-induced partial dehydration of brucite has been confirmed through in-situ electrical conductivity measurements. The partial dehydration reduces the temperature stability of brucite significantly. This mechanism plays a key role in the stability of hydrous minerals in the subducted oceanic slab. In case of the high wetting behavior of the subducted oceanic slab at the transition zone depth, DHMSs are unlikely to serve as water carriers in the transition zone.

Declaration of Competing Interest

The authors declare that they have no known competing financial interests or personal relationships that could have appeared to influence the work reported in this paper.

Acknowledgements

We thank Anhuai Lu and Shuiyuan Yang for their helps in XRD analysis and EPMA analysis, respectively. We also thank Yu Ye for valuable comments. This study was supported by CAS "Light of West China" program (Y9CR026 to X.G.) and the National Natural Science Foundation of China (442072051). This work was also supported by the Ministry of Education, Culture, Sports, Science, and Technology of the Japanese Government, Grant Numbers, 15H05827 and 17H01155 to T.Y.

References

Arcay, D., Tric, E., Doin, M.-P., 2005. Numerical simulations of subduction zones: Effect of slab dehydration on the mantle wedge dynamics. Phys. Earth Planet. Inter. 149 (1-2), 133–153.
Behr, W., Kotowski, M.A.J., Ashley, K.T., 2018. Dehydration-induced rheological heterogeneity and the deep tremor source in warm subduction. Geology 46 (5), 475–478.
Chen, S., Guo, X., Yoshino, T., Jin, Z., Li, P., 2018. Dehydration of phengite inferred by electrical conductivity measurements: implication for the high conductivity anomalies relevant to the subduction zone. Geology 46, 11–14.
de Capitani, C., Petrakakis, K., 2010. The computation of equilibrium assemblage diagrams with Theriak/Domino software. Am. Mineral. 95 (7), 1006–1016.
Fei, Y., Mao, H.-K., 1993. Static compression of $Mg(OH)_2$ to 78 GPa at high temperature and constraints on the equation of state of fluid H_2O. J. Geophys. Res. 98 (B7), 11875–11884.
Ferrand, T.P., Hilairet, N., Incel, S., Deldicque, D., Labrousse, L., Gasc, J., Renner, J., Want, Y., Green, H.W., Schubnel, A., 2017. Dehydration-driven stress transfer triggers intermediate-depth earthquakes. Nat. Commun. 8, 15247.
Freund, F., Wengeler, H., 1980. Proton conductivity of simple ionic hydroxides Part I: the proton conductivities of $Al(OH)_3$, $Ca(OH)_2$, and $Mg(OH)_2$. Ber. Bunsen. Phys. Chem. 84 (9), 866–873.
Fuji-ta, K., Katsura, T., Matsuzaki, T., Ichiki, M., 2007. Electrical conductivity measurements of brucite under crustal pressure and temperature conditions. Earth Planet. Space 59 (6), 645–648.
Gasc, J., Brunet, F., Bagdassarov, N., Morales-Flòrez, V., 2011. Electrical conductivity of polycrystalline $Mg(OH)_2$ at 2 GPa: Effect of grain boundary hydration-dehydration. Phys. Chem. Mineral. 38, 543–556.
Guo, X., Yoshino, T., 2013. Electrical conductivity of dense hydrous magnesium silicates with implication for conductivity in the stagnant slab. Earth Planet. Sci. Lett. 369-370, 239–247.
Guo, X., Yoshino, T., 2014. Pressure-induced enhancement of proton conduction in brucite. Geophys. Res. Lett. 41 (3), 813–819.
Guo, X., Yoshino, T., Katayama, I., 2011. Electrical conductivity anisotropy of deformed talc rocks and serpentinites at 3 GPa. Phys. Earth Planet. Inter. 188 (1-2), 69–81.
Guo, X., Yoshino, T., Shimojuku, A., 2015. Electrical conductivity of albite-(quartz)-water and albite-water-NaCl systems and its implication to the high conductivity anomalies in the continental crust. Earth Planet. Sci. Lett. 412, 1–9.
Hirose, K., Kushiro, I., 1993. Partial melting of dry peridotites at high pressures: determination of compositions of melts segregated from peridotite using aggregates of diamond. Earth Planet. Sci. Lett. 114 (4), 477–489.
Holtzman, B.K., Kohlstedt, D.L., Zimmerman, M.E., Heidelbach, F., Hiraga, T., Hustoft, J., 2003. Melt segregation and strain partitioning: implications for seis-mic anisotropy and mantle flow. Science 301 (5637), 1227–1230.
Hu, H., Dai, L., Li, H., Hui, K., Sun, W., 2017. Influence of dehydration on the electrical conductivity of epidote and implications for high-conductivity anomalies in subduction zones. J. Geophys. Res. 122 (4), 2751–2762.
Hu, H., Dai, L., Li, H., Sun, W., Li, B., 2018. Effect of dehydrogenation on the electrical conductivity of Fe-bearing amphibole: implications for high conductivity anomalies in subduction zones and continental crust. Earth Planet. Sci. Lett. 498, 27–37.
Irving, A.J., Huang, W.L., Wyllie, P.J., 1977. Phase relations of portalandite, $Ca(OH)_2$ and brucite, $Mg(OH)_2$ to 33 kilobars. Am. Jour. Sci. 277, 313–321.
Kanzaki, M., 1991. Dehydration of brucite ($Mg(OH)_2$) at high pressures detected by differential thermal analysis. Geophys. Res. Lett. 18 (12), 2189–2192.
Kempf, E.D., Hermann, J., 2018. Hydrogen incorporation and retention in metamorphic olivine during subduction: implications for the deep water cycle. Geology 46 (6), 571–574.
Li, P., Guo, X., Chen, S., Wang, C., Yang, J., Zhou, X., 2018. Electrical conductivity of the plagioclase–NaCl–water system and its implication for the high conductivity anomalies in the mid-lower crust of Tibet Plateau. Contrib. Mineral. Petrol. 173 (2), 16. https://doi.org/10.1007/s00410-018-1442-9.
Li, Y., Yang, X., Yu, J., Cai, Y., 2016. Unusually high electrical conductivity of phlogopite: the possible role of fluorine and geophysical implications. Contrib. Mineral. Petrol. 171 (4), 37. https://doi.org/10.1007/s00410-016-1252-x.
Liu, X.C., Matsukage, K.N., Li, Y., Takahashi, E., Suzuki, T., Xiong, X.L., 2018. Aqueous fluid connectivity in subducting oceanic crust at the mantle transition zone conditions. J. Geophys. Res. 123 (8), 6562–6573.
Ma, M., Liu, W., Chen, Z., Liu, Z., Li, B., 2013. Compression and structure of brucite to 31 GPa from synchrotron X–ray diffraction and infrared spectroscopy studies. Am. Mineral. 98 (1), 33–40.
Manthilake, G., Bolfan-Casanova, N., Novella, D., Mookherjee, M., Andrault, D., 2016. Dehydration of chlorite explains anomalously high electrical conductivity in the mantle wedges. Sci. Adv. 2, (5) e1501631.

Manthilake, G., Mookherjee, M., Bolfan-Casanova, N., Andrault, D., 2015. Electrical conductivity of lawsonite and dehydrating fluids at high pressures and temperatures. Geophys. Res. Lett. 42 (18), 7398–7405.
Matsukage, K.N., Hashimoto, M., Nishihara, Y.u., 2017. Morphological stability of hydrous liquid droplets at grain boundaries of eclogite minerals in the deep upper mantle. J. Miner. Petrol. Sci. 112 (6), 346–358.
Mibe, K., Fujii, T., Yasuda, A., 1999. Control of the location of the volcanic front in island arcs by aqueous fluid connectivity in the mantle wedge. Nature 401 (6750), 259–262.
Mibe, K., Fujii, T., Yasuda, A., 1998. Connectivity of aqueous fluid in the Earth's upper mantle. Geophys. Res. Lett. 25 (8), 1233–1236.
Mibe, K., Yoshino, T., Ono, S., Yasuda, A., Fujii, T., 2003. Connectivity of aqueous fluid in eclogite and its implications for fluid migration in the Earth's interior. J. Geophys. Res. 108 (B6), 2295. https://doi.org/10.1029/2002JB001960.
Nakao, A., Iwamori, H., Nakakuki, T., 2016. Effects of water transportation on subduction dynamics: roles of viscosity and density reduction. Earth Planet. Sci. Lett. 454, 178–191.
Ohtani, E., Toma, M., Litasov, K., Kubo, T., Suzuki, A., 2001. Stability of dense hydrous magnesium silicate phases and water storage capacity in the transition zone and lower mantle. Phys. Earth Planet. Inter. 124 (1-2), 105–117.
Ono, S., Mibe, K., Yoshino, T., 2002. Aqueous fluid connectivity in pyrope aggregates: water transport into the deep mantle by a subducted oceanic crust without any hydrous minerals. Earth Planet. Sci. Lett. 203 (3-4), 895–903.
Palot, M., Jacobsen, S.D., Townsend, J.P., Nestola, F., Marquardt, K., Miyajima, N., Harris, J.W., Stachel, T., McCammon, C.A., Pearson, D.G., 2016. Evidence for H_2O-bearing fluids in the lower mantle from diamond inclusion. Lithos 265, 237–243.
Pearson, D.G., Brenker, F.E., Nestola, F., McNeill, J., Nasdala, L., Hutchison, M.T., Matveev, S., Mather, K., Silversmit, G., Schmitz, S., Vekemans, B., Vincze, L., 2014. Hydrous mantle transition zone indicated by ringwoodite included within diamond. Nature 507 (7491), 221–224.
Perrillat, J., Daniel, I., Koga, K., Reynard, B., Cardon, H., Crichton, W., 2005. Kinetics of antigorite dehydration: a real-time X-ray diffraction study. Earth Planet. Sci. Lett. 236 (3-4), 899–913.
Peters, D., Pettke, T., John, T., Scambelluri, M., 2020. The role of brucite in water and element cycling during serpentinite subduction- Insights from Erro Tobbio (Liguria, Italy). Lithos 360–361, 105431. https://doi.org/10.1016/j.lithos.2020.105431.
Schmandt, B., Jacobsen, S.D., Becker, T.W., Liu, Z., Dueker, K.G., 2014. Dehydration melting at the top of the lower mantle. Science 344 (6189), 1265–1268.
Schramke, J.A., Kerrick, D.M., Blencoe, J.G., 1982. Experimental determination of the brucite = periclase + water equilibrium with a new volumetric technique. Am. Mineral. 67, 269–276.
Shinoda, K., Yamakata, M., Nanba, T., Kimura, H., Moriwaki, T., Kondo, Y., Kawamoto, T., Niimi, N., Miyoshi, N., Aikawa, N., 2002. High-pressure phase transition and behavior of protons in brucite $Mg(OH)_2$: a high-pressure-temperature study using IR synchrotron radiation. Phys. Chem. Mineral. 29 (6), 396–402.
Syracuse, E.M., van Keken, P.E., Abers, G.A., 2010. The global range of subduction zone thermal models. Phys. Earth Planet. Inter. 183 (1-2), 73–90.
van Aken, P.A., Langenhorst, F., 2001. Nanocrystalline, porous periclase aggregates as product of brucite dehydration. Eur. J. Mineral. 13 (2), 329–341.
Wang, D., Guo, Y., Yu, Y., Karato, S.-I., 2012. Electrical conductivity of amphibole-bearing rocks: influence of dehydration. Contrib. Mineral. Petrol. 164 (1), 17–25.
Watson, E.B., Brenan, J.M., Baker, D.R., 1991. Distribution of fluids in the continental mantle. In: Menzies, M. (Ed.), Continental Mantle. Oxford University Press, pp. 111–125.
Yoshino, T., Nishihara, Y.u., Karato, S.-I., 2007. Complete wetting of olivine grain boundaries by a hydrous melt near the mantle transition zone. Earth Planet. Sci. Lett. 256 (3-4), 466–472.
Zhang, B., Guo, X., Yoshino, T., Xia, Q., 2021. Electrical conductivity of melts: Implications for conductivity anomalies in the Earth's mantle. Natl. Sci. Rev. 8, nwab064. https://doi.org/10.1093/nsr/nwab064.
Zhang, B., Yoshino, T., Yamazaki, D., Manthilake, G., Katsura, T., 2014. Electrical conductivity anisotropy in partially molten peridotite under shear deformation. Earth Planet. Sci. Lett. 405, 98–109.
Zheng, H., Xie, H., Xu, Y., Song, M., Guo, J., Zhang, Y., 1997. The electrical conductivity of H_2O at 0.21-4.18 GPa and 20–350 degrees C. Chin. Sci. Bull. 42 (12), 969–976.